8
How Protein Motors Convert Chemical Energy into Mechanical Work

George Oster and Hongyun Wang

'Biologists observe things that cannot be explained. Theorists explain things that cannot be observed'.

Aharon Katchalsky

8.1
Introduction

Imagine living in a world where a Richter 9 earthquake raged continuously. In such an environment, engines would be unnecessary. You would not need to even pedal your bicycle: you would simply attach a ratchet to the wheel preventing it from going backwards and shake yourself forwards! At the scale of proteins, Brownian motion is even more furious, and proteins evolved to take advantage of this enormous supply of energy. Feynman showed that the familiar mechanical ratchet could not work in an isothermal environment, lest it violate the Second Law of Thermodynamics (Feynman et al., 1963), and so motor proteins must employ a different strategy to convert random thermal fluctuations into a directed force: they use chemical energy via intermolecular forces to capture 'favorable' configurations. The way in which proteins do this is dictated by three factors: their size, the strength and range of intermolecular bonds at physiological conditions and the magnitude of the Brownian fluctuations that constitute their thermal environment. These determine the energy, length and time scales on which protein motors can operate.

Roughly speaking, motor proteins trap thermal fluctuations in two ways: by biasing diffusion of small, angstrom-sized, steps ('small ratchets'), and by rectifying nanometer-sized or larger, diffusional displacements ('big ratchets'). For reasons that will become clear, biasing a sequence of small Brownian fluctuations is generally called a *power stroke*, while rectifying a large thermal displacement is called a *Brownian ratchet*. Said another way, Brownian ratchets move down free energy landscapes in steps much larger than k_BT, while power strokes move in steps comparable to or smaller than k_BT.[1)] The distinction is imprecise, but useful, since it

1) The quantity k_BT measures the thermal energy of Brownian motion; its value is $1\ k_BT \sim 4.1$ pN nm $= 4.1 \times {}^{10\text{-}21}$ J at 298 K (25 °C).

delineates two extremes in the general mechanism by which proteins use intermolecular attractions to convert chemical energy into mechanical work.[1)]

There are only a few motors that can be regarded as being pure power stroke motors or pure ratchets; most protein motors employ a combination of the two strategies. However, these 'thoroughbreds' are good illustrations of the principles. In fact, evolution has designed one protein that joins both ratchet and power stroke motors into one remarkable device: F_0F_1 ATPase, or ATP synthase, the machine that manufactures the fuel that powers many other protein machines. We will use this protein as our running example.

Since this volume is aimed primarily at biologists, our discussion will be mostly qualitative and heuristic. However, it is important to realize that the explanatory cartoons we use are supported by extensive calculations. Omitting them is akin to leaving out the 'Materials and Methods' section in an experimental paper: assertions without authority are simply opinions. The supporting quantitative arguments are, perforce, contained in the citations.

8.2
A Brief Description of ATP Synthase Structure

In order to discuss the workings of the F_0 and F_1 motors we give a brief account of their structure, which is summarized in Fig. 8.1. A more complete account is given in Chapter 5 by Noji in this volume. ATP synthase comprises two rotary motors acting in opposition, each operating on an entirely different physical mechanism. The F_0 motor is contained in the membrane-bound portion and employs as its energy source a transmembrane electromotive force. The F_1 motor is contained in the soluble portion and is driven by the hydrolysis of ATP.

The F_1 motor is constructed of a coiled-coil shaft (the γ-subunit) surrounded by a hexamer composed of alternating α and β subunits. Nucleotide binding sites nestle in the cleft between subunits; however, only three of the sites are catalytically active, the other three bind, but do not hydrolyze, ATP. The catalytic sites are contained mostly in the β-subunit, with a few – but crucial – residues contributed by the α subunit. The catalytic sites hydrolyze sequentially and drive the rotation of the γ-shaft. Movies showing the motion of the hexamer and the rotation of the γ-shaft can be downloaded from a web site given in (Oster and Wang, 2000a; Wang and Oster, 1998).

The F_0 motor is composed of two portions. Between 10 and 14 c-subunits (depending on the species and/or conditions) are assembled into a cylinder attached to the γ-shaft and ε-subunit. It interfaces with a second transmembrane assembly consisting of the a and b subunits. By convention, the $\gamma\text{-}c_n\text{-}\varepsilon$ assemblage is called the 'rotor', and the remainder of the protein (the $\alpha_3\beta_3$ hexamer and the $\delta\text{-}\beta_2$-a complex) comprises the 'stator', although each rotates in the opposite direction.

1) We have included a short Appendix with several simple examples that illustrate the difference between a 'power stroke' and a 'Brownian ratchet'.

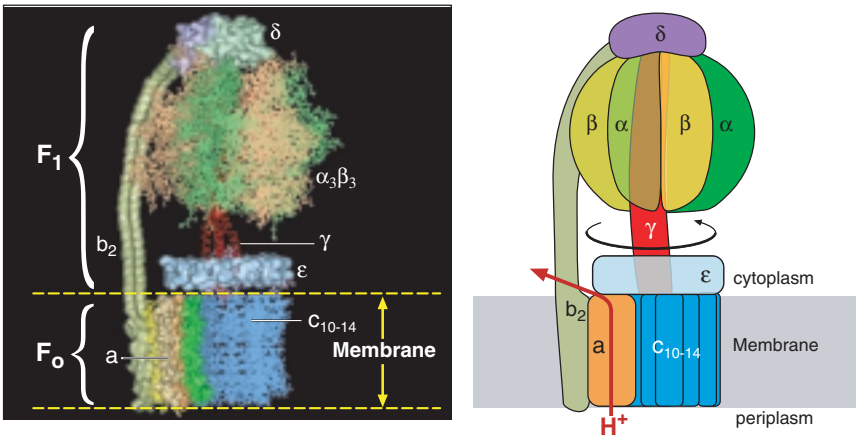

Figure 8.1. The structure of ATP synthase. The panel on the left shows a composite based on the pdb coordinates of the known subunits (Pedersen et al., 2000); the right-hand panel is the corresponding structure represented schematically showing the relative rotation of the F_0 and F_1 motors and the direction of ion flow through the a-cn subunit interface. Subscripts denote the subunit stoichiometries.

8.3
The F1 Motor: A Power Stroke

The study of protein ATPases has led to a few generalizations that help us understand the mechanism by which these molecular motors convert the energy residing in the nucleotide γ-phosphate bond into a directed mechanical force.

- At physiological conditions, the free energy of hydrolysis of one ATP is $\sim$ 20–24 k_BT; of this, about 8–9 k_BT is enthalpic, the balance being entropic.
- Almost all nucleotide binding sites are nestled in the cleft between protein subunits. The nucleotide is grasped by loops emanating from a parallel β-sheet.
- In many motors, the force-generating step is associated with the binding of nucleotide to the catalytic site. *We propose that this is true of all ATPase motors.* In particular, for the F_1 motor this is the only way to reconcile all of the biochemical and mechanical measurements with its high mechanical efficiency.
- After the force has been generated by ATP binding, an ATP is tightly bound in the catalytic site. The role of hydrolysis is to break the tightly bound ATP into two products and weaken the binding so the products can be released and the force-generating cycle can be repeated.

In the F_1 motor, the ATP binding site lies asymmetrically in the cleft between the β and α subunits, the majority of the catalytic sites residing in the β subunit. The power stroke is accomplished by a hinge bending motion that swings the top of the β subunit down towards the bottom portion. The bending motion of the β subunit can be measured by the motion of helices B and C that emanate from the β

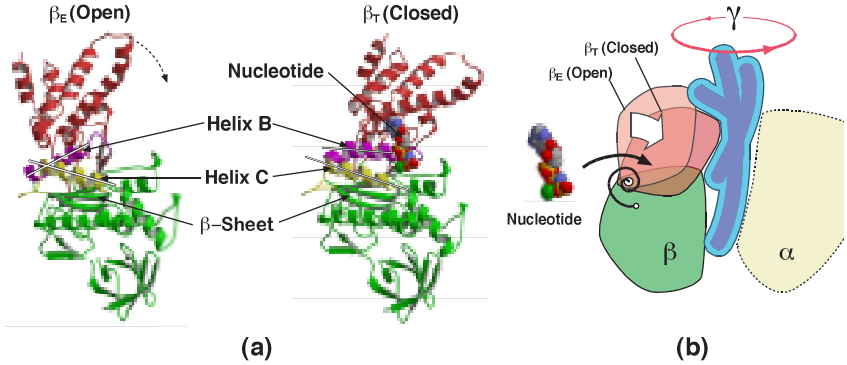

Figure 8.2. The F_1 power strokes are accomplished by the hinge bending motions of β subunits, which are driven by ATP binding to the catalytic sites. (a) During the hinge bending motion, the top part of β rotates about 30° toward the bottom part. This rotation closes the angle between helices B and C. (b) The hinge bending motion of each β subunit pushes on the off-axis section of the γ shaft. The rotation of the γ shaft is driven by the coordinated hinge bending motions of all three β subunits (Oster and Wang, 2000, Wang and Oster, 1998).

sheet of the catalytic site, as shown in the ribbon diagram in Fig. 8.2a. The bending of the β subunit by about 30° rotates the central γ shaft by pushing on its off-axis section, much like turning a crankshaft (Fig. 8.2b).

The energy for the power stroke derives from the nucleotide hydrolysis cycle, which consists of four major steps:

$$\begin{aligned} &CS + ATP \underset{1}{\overset{\text{Binding}}{\rightleftharpoons}} CS \bullet ATP \underset{2}{\overset{\text{Hydrolysis}}{\rightleftharpoons}} CS \bullet ADP \bullet P_I \\ &P_I \underset{3}{\overset{\text{Release}}{\rightleftharpoons}} CS \bullet ADP + P_I \underset{4}{\overset{\text{ADP Release}}{\rightleftharpoons}} CS + ADP \end{aligned} \tag{8.1}$$

The nucleotide binding step 1 is the force-generating step and should more properly be expressed as a sequence of binding steps:

$$CS + ATP \rightleftharpoons CS \cdot ATP \rightleftharpoons \cdots \rightleftharpoons \underbrace{CS \bullet ATP}_{\text{Binding Transition}} \tag{8.2}$$

Here the progression from weak to tight binding is symbolized by the increasing size of the bonding symbol indicating the progressive annealing of 15–20 hydrogen bonds (and some hydrophobic interactions at the sugar end). The mechanism driving the hinge bending motion of the β is illustrated schematically in Fig. 8.3. Immediately after it diffuses into an open and loose catalytic site, the ATP is bound only weakly. The catalytic site wraps around the ATP by forming more bonds which

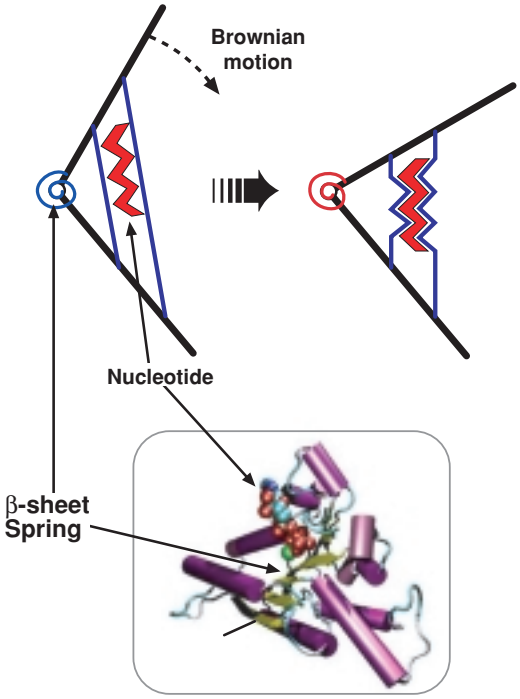

Figure 8.3. The ATP binding transition from weak to tight proceeds as the catalytic site grasps the ATP in a grip of hydrogen bonds (the 'binding zipper'). As binding progresses, the catalytic site closes up and pulls the top part of the β subunit toward the bottom part. In this way, the binding free energy is converted to a power stroke with nearly a constant force. During the power stroke some of the binding energy is stored in the elastic deformation of the β-sheet, which acts like a spring. This energy is released during the unbending motion to aid product release and return the subunit to its open state.

tightens the catalytic site and pulls down the top part of β toward the bottom part. The bonds between the ATP and the catalytic site are formed more or less sequentially, the formation of each bond corresponding to a small drop in binding free energy, that drives a small fraction of the hinge bending motion (Bockmann, 2002, Oster and Wang, 2000a; Sun et al., 2002). When all the bonds have been formed, the ATP is tightly bound at the catalytic site. The overall process from weak to tight binding is called the 'binding transition'. During the binding transition, the ATP binding free energy is utilized efficiently to generate a bending motion with a nearly constant torque about the hinge region near the β-sheet.

The binding transition has two important features (Oster and Wang, 2000a,b, Sun et al., 2002):

- The binding free energy decreases (the binding becomes stronger) nearly monotonically and smoothly during the binding transition. This drives the hinge bending motion of the β subunit and consequently the γ shaft rotation in the hydrolysis cycle. In the reverse synthesis cycle, the unbending of the β subunit is driven by the γ shaft rotation in the opposite direction, powered by the F_0 motor. When the top of the β subunit is forced up and away from the bottom portion, the binding free energy increases (the binding becomes weaker). This progressively releases the nucleotide from the catalytic site.

- By the end of the binding transition, approximately 6–10 k_BT of elastic energy is stored in the β-sheet whose loops grasp the nucleotide. Note that the catalytic site should be flexible but not elastic, lest it dissipate too much of the binding free energy by elastic recoil.

To summarize, the power stroke is driven by progressive capturing of relatively small Brownian motions that anneal the nucleotide into the catalytic site. Product release is accomplished by using the free energy of hydrolysis to weaken the product binding so that thermal fluctuations can knock them out of the catalytic site. Thus Brownian motion drives both the power and exhaust strokes.

8.4 The F_0 Motor: A Brownian Ratchet

The F_0 motor is driven by the ion-motive force, $\Delta\mu_c$ across a bacterial or mitochondrial inner membrane. The ion-motive force consists of an ion concentration gradient and an electrical potential difference. In most organisms, the ion is a proton. However, much information has been gleaned from anaerobic bacteria whose F_0 is driven by a sodium ion motive force. In either case, the transmembrane chemical potential difference in millivolts is given by:

$$\Delta\mu_{c^+} = 2.3\left(\frac{k_BT}{e}\right)\underbrace{\left(\log_{10}[c^+]_p - \log_{10}[c^+]_c\right)}_{\Delta pH} + \Delta\psi \qquad [mV] \tag{8.3}$$

where e is the electronic charge, $[c^+]_p$ the ion (sodium or proton) concentration of the periplasm expressed in molars, $[c^+]_c$ the ion concentration of the cytoplasm and $\Delta\psi$ is the electrical potential difference across the membrane. Equation 8.3 is a thermodynamic relationship that implies that a concentration difference is equivalent to an electrical potential at equilibrium. Since motors operate out of equilibrium, this turns out not to be true in general. However, Eq. 8.3 points out the need for a mechanism for transforming both an entropic and electrical potential into mechanical work. The basic principle that accomplishes this can be illustrated by the 'toy' model shown in. Fig. 8.4.

8.4.1 A Pure Brownian Ratchet

First, consider a rod with a linear array of negative charges (e. g. a DNA strand, etc.) that can freely diffuse through a hydrophilic pore embedded in a membrane as shown in Fig. 8.4a. If a potential, $\Delta\psi$, is imposed across the membrane, then the rod will be propelled to the left and can perform work against a load force, F_L. This can be considered as nearly a pure power stroke. The motion of the rod can be viewed as being driven by a driving potential, ϕ, tilted to the left in Fig. 8.4a. The slope of the driving potential gives the motor force driving the rod

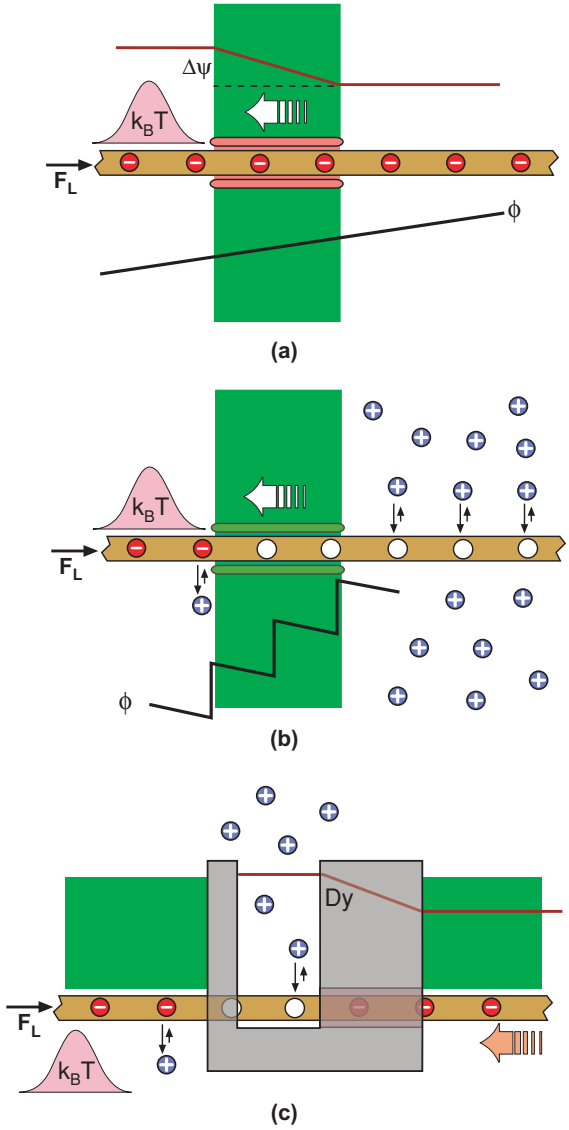

Figure 8.4. Principle of the F_0 motor. (a) A pure power stroke. A rod of negative electrical charges passes through a polar transmembrane pore (colored white). An electrical potential, Δψ imposed across the membrane drives the line of charges to the left. (b) A pure Brownian ratchet. The charged rod passes through a hydrophobic membrane pore (colored gray). A high concentration of counter-ion charges (Na^+ or H^+) on the right can bind to the negative sites and neutralize them so that they can pass through the pore. A second positive ion on the left (not shown) neutralizes the membrane potential. The low concentration of counter-ions on the left ensures that the bound charges dissociate but do not quickly rebind, so that the bare site cannot re-enter the pore. The attractive bonds between the rod charge and the aqueous solvent molecules rectify the rod's diffusion. We call this a Brownian ratchet. (c) The power stroke and ratchet can be combined using an L-shaped 'stator'. An aqueous input channel (colored white) connects via a polar channel (colored white) to the output reservoir. The body of the stator is hydrophobic so that ions cannot leak across the membrane. With this design, the motor has both power stroke and ratchet components.

to the left: $F_M = - d\phi/dx$. The rod will stall when the motor force equals the load force: $F_M = F_L$. Because the rod is very small, its motion is stochastic (indicated in Fig. 8.4 by the Gaussian force labeled k_BT). In fact, the net drift of the rod driven by the potential is deeply buried in its random motion: at any time the rod is only a tiny bit more likely to move to the left than to the right, and the mean square of the instantaneous velocity is several orders of magnitude larger than the net drift velocity. So the net movement down the potential gradient can only be detected

by looking at correlations over many steps. This is illustrated by example 3 in the Appendix.

8.4.2 A Pure Power Stroke

Next, consider the situation in Fig. 8.4b where the rod passes through a hydrophobic pore. Moreover, there is a difference in the concentration of a positive counterion (e. g. sodium or protons) between the two sides of the membrane. The counterion can bind to and neutralize the negative charges (binding sites) on the rod. A difference in the concentration of a second ion (e. g. potassium), which cannot bind to the sites on the rod, neutralizes the membrane potential. A bare binding site is negatively charged and cannot move into the hydrophobic pore, for that would entail shedding its hydration shell at a considerable energetic cost.[1)] Because of the high concentration on the right side, the binding sites will be largely neutralized and so the rod can diffuse freely to the left through the pore. However, once a neutralized site has emerged from the pore to the left, the bound positive charge will quickly dissociate and leave the binding site unoccupied. Because of the low concentration on the left side, the binding site is likely to remain unoccupied, which prevents it from moving back into the pore. Thus diffusion to the right is rectified by the ion concentration difference, and the rod moves stochastically to the left, driven by a pure Brownian ratchet. The driving potential, ϕ, in this case looks like a staircase. When the concentration on the left is much lower than that on the right, each step of the staircase potential is much larger than k_BT, so that reverse steps are unlikely. This is illustrated by example 4 in the Appendix. The load force, F_L, opposing the motion has the effect of 'tilting' the driving potential so that the rod must diffuse uphill, against the load force.

The two driving forces can be combined as shown in Fig. 8.4c. Here the membrane is horizontal and so the motor must be augmented by a fixed 'stator' assembly. The stator body is hydrophobic with two exceptions. First, there is a large aqueous channel that permits the ions from the high concentration reservoir to access the binding sites. Second, there is a polar channel connecting the aqueous channel to the low concentration reservoir. Since the aqueous channel is isopotential with the high concentration reservoir, this arrangement converts the transmembrane potential drop from vertical to horizontal. In this way the membrane potential and the ion concentration difference act in tandem to move the rod to the left, the former driving a power stroke and the latter driving a Brownian ratchet.

The actual F_0 motor works somewhat differently from the idealized version in Fig. 8.4c. Fig. 8.1a shows two more modifications that are required to make the arrangement resemble the sodium driven F_0 motor of the bacterium *P. modestum* (Dimroth et al., 1999, Oster et al., 2000). The linear array of charged binding sites is first wrapped around a cylinder This cylinder consists of 10−14 c-subunits,

1) The energy cost of moving a negative charge into the pore is approximately $\Delta G \approx 45\ k_BT$ (Israelachvili and Ninham, 1977).

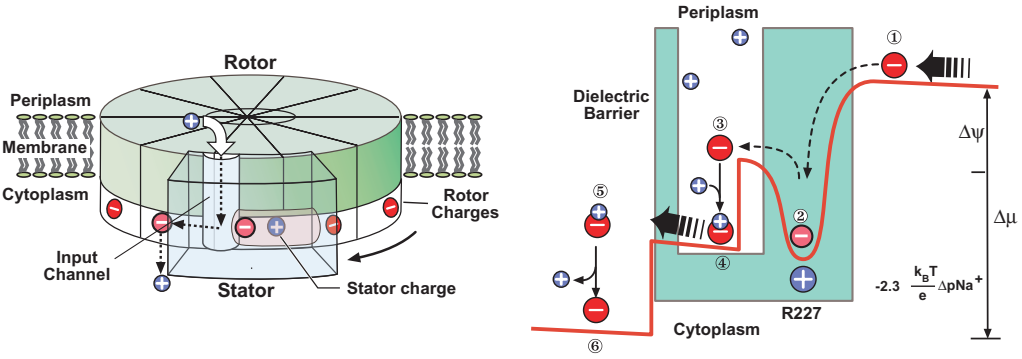

Figure 8.5. Operation of the F_0 motor (Dimroth et al., 1999). (a) Simplified geometry of the sodium driven F_0 motor showing the path of ions through the stator. This is the same arrangement as in Fig. 8.4c, but with the charge array wrapped around a cylinder that is free to rotate in the plane of the membrane with respect to the stator. In addition, a 'blocking charge' has been added to the stator to prevent the leakage of charge from the high concentration reservoir (periplasm) to the low concentration reservoir (cytoplasm). (b) Free energy diagram of one rotor site as it passes through the rotor–stator interface. Step 1 → 2, the rotor diffuses to the left, bringing the empty (negatively charged) site into the attractive field of the positive stator charge. 2 → 3, once the site is captured, the membrane potential biases the thermal escape of the site to the left (by tilting the potential and lowering the left edge). 3 → 4, the site quickly picks up an ion from the input channel neutralizing the rotor. 4 → 5, an occupied site being nearly electrically neutral can pass through the dielectric barrier. If the occupied site diffuses to the right, the ion quickly dissociates back into the input channel as it approaches the stator charge. 5 → 6, upon exiting the stator the site quickly loses its ion. The empty (charged) site binds solvent and cannot pass backwards into the low dielectric of the stator. The cycle decreases the free energy of the system by an amount equal to the electromotive force.

depending on the organisms and/or conditions. Second, a 'blocking charge' (R232) is present on the stator that prevents leakage of ions between the two reservoirs that would dissipate the ion gradient unproductively. The presence of this blocking charge alters the picture of the rotation of the rotor with respect to the stator substantially. Fig. 8.1b shows the potential experienced by one binding site of the F_0 motor. The presence of the blocking charge creates an electrostatic potential well that attracts the rotor binding site as soon as it diffuses into the polar channel. Once trapped in the well, the rotor depends on Brownian fluctuations to escape. However, the membrane potential biases escape by lowering the left side of the electrostatic well so that the rotor charge is much more likely to escape to the left than to the right. Once it escapes into the aqueous input channel, it is quickly neutralized by the positive ions so that it can move freely across the hydrophobic barrier. Note that the membrane potential only biases the Brownian fluctuations to the left, but does not actually drive a power stroke as in Fig. 8.4a.

In summary, the F_0 motor qualifies as a Brownian ratchet since it rectifies large thermal fluctuations (or long diffusions). The energy for rectification derives from the ion concentration gradient via the short range interactions between ions and

the binding sites (binding and unbinding). It also uses the membrane potential to bias thermal fluctuations that release the rotor site from the attraction of the stator blocking charge: it takes less energy to hop out to the left than to the right. This might be thought of as a partial power stroke, so we see that the classification into power stroke and ratchet is largely a question of definition.

An interesting class of ratchet motors is those that use the principle of trapping Brownian fluctuations during their assembly to perform a '1-shot' motor task. Examples include the acrosome of *Limulus* and *Thyone*, the spasmoneme of *Vorticella* (Mahadevan and Matsudaira, 2000), and the polymerizaton of actin that propels lamellipodial protrusion and certain intracellular parasites, such as *Listeria* and *Shigella* (Mogilner and Oster, 1996a,b).

An important corollary of the ratchet principle, and one that dramatically distinguishes molecular motors from other machines, is that using thermal fluctuations to go uphill in free energy amounts cools off the immediate environment. If the ratchet shown in Fig. 8.4b is coupled to work against a conservative load force, then the process is endothermic: heat is absorbed from surrounding fluid to increase the potential energy of the external agent that exerts the load force. By contrast, if the motor shown in Fig. 8.4a is coupled to work against a viscous load, then the process is exothermic: energy from the electrical potential goes to produce the drift velocity of the rod, which in turn is converted to heat by viscous friction. These microscopic thermal energy transactions lead to some surprising properties of molecular motors. For example, it is possible for the motor to perform more work on a *viscous* load than the free energy it derives from a reaction cycle! These counterintuitive properties are discussed in more detail in the references (Oster and Wang, 2000b, Wang and Oster, 2001).

8.5
Coupling and Coordination of Motors

Most ATPase motors have more than one catalytic site. During the motor operation, each catalytic site hydrolyzes ATP and contributes to force generation. These catalytic sites generally do not operate independently, but act in concert with other catalytic sites. Two heads of a kinesin dimer are coordinated with each other to generate unidirectional motion and to ensure processivity. ATP synthase has three catalytic sites. AAA motors are hexamers of ATPases, sometimes stacks of two hexamers. The chaperonin Groel is a stacked pair of heptameric rings, each with seven catalytic sites and the portal protein may even be a dodecameric ring of 12 ATPases. Generally, the catalytic sites must act in concert, either firing sequentially, as in F_1, or as in Groel, simultaneously in each ring, but alternating between the rings. This coordination is necessary for the proper operation of the motors, but how is it accomplished?

In all cases, motor ATPase catalytic sites are too far apart to communicate in any other way than via elastic strain through the intervening protein structure. Although the details of strain coordination differ, a clue can be found in the correla-

tion between the ADP release at one catalytic site and the ATP binding at another. In F_1, the strain-induced release of ADP arises from two possible sources. First, the γ shaft is asymmetric, so that at every rotational position it strains each catalytic site differently. Second, the intrinsic asymmetry of the protein structure allows the catalytic site to radiate strain differently to the two neighbor sites. The catalytic sites are located in the cleft between adjacent α and β subunits, with the majority of the binding residues in the β subunit (Menz et al., 2001, Stock et al., 2000). This asymmetry allows ATP binding at one catalytic site to propagate a conformational change to the β portion of next catalytic site in the direction of motor rotation, but propagates a different conformational change to the α portion of the previous catalytic site. Thus, one catalytic site can affect the reactions on two neighboring catalytic sites differently. The conformational change directed to the β portion of the next catalytic site can lower the free energy barrier for ADP dissociation, readying it for the next hydrolysis cycle. Indeed this may be the primary structural feature determining the direction of rotation.

Because of the unequal symmetry between the F_0 and F_1 motors, elastic coupling plays an additional role. The F_1 motor has three catalytic sites and rotates in three major 120° steps, each with a brief pause at 90°. On the other hand, the F_0 motor has a rotational symmetry that varies between 10 and 14, depending on the source. Therefore, there is no unique 'stoichiometry' between the two rotational motions. This symmetry mismatch is not a problem for the motors since the γ-shaft that couples them is torsionally flexible. In synthesis, this allows the stochastic F_0 motor to deliver a smooth torque to F_1, which minimizes dissipation as the nucleotide is unzipped from the catalytic site (Junge et al., 2001; Oster and Wang, 2000a). Thus elastic coupling between subunits of a protein motor provides the means for both coordinating the catalytic cycles and buffering the independent Brownian motions of the subunits.

In walking motors the determination of directionality depends on asymmetric structural features of the heads that alternate depending on whether the head is leading or trailing. However, the situation is more complicated since each head has two binding partners: nucleotide and track. One proposal is that strain is generated by binding of the forward head to the track, triggers release of product from that head (Uemura et al., 2002). Also strain is relayed to the rear head via the connecting structure to lower the energy barrier for a particular step in the reaction cycle (for example, hydrolysis, or product release). This particular reaction step, in turn, triggers the release of rear head from the track (Hancock and Howard, 1999). Thus, binding to and release from the track are correlated with the relative positions of the heads. The alternating phases of the two hydrolysis cycles generate unidirectional motion (Peskin and Oster, 1995).

8.6 Measures of Efficiency

We have discussed the molecular principles by which protein motors convert chemical bond energy into mechanical work. However, while the general principles may be the same for all motors, the detailed mechanisms are quite diverse. Therefore, it is frequently useful to determine the efficiency of a motor to provide clues as to its mechanism.

The most common mechanical measurement performed on protein motors is to vary the load (the force resisting the motion) and measure the speed. In general, two kinds of load experiments are carried out on protein motors in order to determine their load–velocity behavior. In one type, a load is applied to resist the motor's progress using a laser trap or the elastic stylus of an atomic force microscope. In this case the motor is working against a *conservative* force (i. e. derivable from a potential energy function) that depends only on the *displacement* of the motor, $f = -\partial\phi/\partial\xi$). A second, and generally more experimentally convenient method, is to vary the viscous resistance of the fluid environment of the motor. This is a *dissipative* force that depends on the motor *velocity*. The information gleaned from the two kinds of measurements yield different information (Oster and Wang, 2000a, Wang and Oster, 2002a,b).

The *thermodynamic efficiency*, η_{TD}, is generally defined as the ratio of the work done by the motor to the energy input:

$$\eta_{TD} = \frac{f \cdot \langle \delta \rangle}{-\Delta G} \tag{8.4}$$

where ΔG is the free energy drop in one reaction cycle (e. g. from hydrolyzing one ATP, or passing one proton through the motor), and $f\cdot\langle\delta\rangle$ is the reversible work done by the motor against the conservative load force, f, in one reaction cycle. Here $\langle\delta\rangle$ is the average distance covered per reaction cycle, sometimes called the 'step size'. $f\cdot\langle\delta\rangle$ is the energy output from the motor because it goes to increasing the potential energy of the external agent that exerts the conservative force. Thus, the thermodynamic efficiency is the ratio of energy output to energy input and it measures the energy conversion efficiency when the motor is operating reversibly, i. e. 'infinitely slowly'.

For a motor working against a constant force (e. g. a laser trap force clamp), Eq. 8.4 can be generalized to the steady state (Oster and Wang, 2000a, Wang and Oster, 2002b) by defining an efficiency:

$$\eta \equiv \frac{f \cdot \langle v \rangle}{-\Delta G \cdot \langle r \rangle} \tag{8.5}$$

Here $\langle r\rangle$ is the average reaction rate (e. g. hydrolysis cycles per second or average proton flux) and $\langle v\rangle$ is the average velocity. Strictly speaking, Eq. 8.5 is not a thermodynamic quantity since the steady state need not be the equilibrium state. Nevertheless, it is a well-defined quantity that is less than unity.

In general, the average step size, $\langle\delta\rangle$ depends on the load force, f. When $\langle\delta\rangle$ is *independent* of f, we say the motor is *tightly coupled*. In that case, each reaction cycle is, on average, coupled to a fixed displacement (one motor step) regardless of the load force. A tightly coupled motor has two properties:

- When the motor is stalled the chemical reaction is also stopped.
- Increasing the load beyond the stall force drives the motor in the opposite direction and also reverses the chemical reaction.

For a tightly coupled motor, one can show that the stall force is given by $f_{stall} = -\Delta G/\langle\delta\rangle$. At stall, the thermodynamic efficiency is 100 %. When the motor is operating close to stall, the thermodynamic efficiency approaches 100 %, regardless of the motor mechanism. *Conversely, a high thermodynamic efficiency suggests only that the motor motion and the chemical reaction are tightly coupled* (Wang and Oster, 2002a).

Equation 8.5 applies only to the situation where the motor is working against a constant load. For macroscopic motors, inertia is important and the effect of Brownian fluctuations is negligible. Therefore, they tend to move at roughly a constant velocity (at least on short time scales), and so the friction force on the motor is approximately constant. In this case, the friction force can be treated effectively as a conservative force and the efficiency given by Eq. 8.5 is well defined. Thus, for a macroscopic motor, we generally do not have to worry whether it is working against a conservative force or a friction force. That is, for a macroscopic motor moving with roughly a constant velocity, both a viscous drag and a conservative load simply oppose the motor motion and they have approximately the same effect on the motor. *For a protein motor, the situation is very different*. Because protein motors are very small, the effect of inertia is negligible and the motor is driven mostly by the random Brownian force. The instantaneous velocity changes direction very rapidly and its absolute value is several orders of magnitude larger than the average velocity. Consequently, the drag force on the motor is stochastic and cannot be treated as a conservative force. The effect of a conservative load force on the motor is different from that of a viscous drag force that simply opposes the motor motion in any direction and whose magnitude increases with the velocity.[1)] *Therefore, for protein motors, it is necessary to distinguish the case where the motor is loaded with a conservative force and the case where the motor is loaded with a viscous drag.*

When a protein motor works against a viscous load, the thermodynamic efficiency defined above does not apply. A commonly employed measure of efficiency in this case is the *Stokes efficiency,* defined by replacing f in Eq. 8.5 with the average viscous drag force, $f_D = \zeta\langle v\rangle$. Here $\zeta = k_BT/D$ is the drag coefficient and D is the diffusion coefficient, which can be computed or measured independently (Wang and Oster, 2002a):

1) A conservative load force tends to drive the motor backwards (opposite to the positive motor direction) and its magnitude is independent of the velocity. A viscous drag simply damps the motor velocity, while the Brownian force and/or the chemical reaction excite the velocity. If the chemical reaction is halted, the viscous drag will relax the motor to thermal equilibrium with the surrounding fluid, while the conservative force will drive the motor in the opposite direction.

$$\eta_{Stokes} = \frac{\zeta\langle v\rangle\langle\delta\rangle}{-\Delta G}, \text{ or } \eta_{Stokes} = \frac{\zeta\langle v\rangle^2}{-\Delta G\cdot\langle r\rangle} \tag{8.6}$$

Although $\zeta\langle v\rangle^2$ has the dimension of energy per unit time, $\zeta\langle v\rangle^2$ *is not the rate of the work done by the motor motion on the fluid medium*[1]. Indeed, it is not clear what energy per unit time $\zeta\langle v\rangle^2$ measures. However, since $\zeta\langle v\rangle^2$ increases with $\langle v\rangle$, the quantity $\zeta\langle v\rangle^2$ does measure some aspect of the motor's mechanical performance. So the Stokes efficiency is the ratio of this 'mechanical performance' index to the energy supply. Of course, for Eq. 8.6 to be a valid measure of efficiency, it has to satisfy $\eta_{Stokes} \leq 100\,\%$. This is true, but the proof is not trivial. One can show that *Eq. 8.6 measures how close the motor comes to delivering a constant force* (Oster and Wang, 2000a, Wang and Oster, 2002a,b). Given the free energy supply $-\Delta G$, the maximum average velocity is achieved if $-\Delta G$ is utilized to generate a roughly constant driving force (independent of motor position). When the driving force is constant, the Stokes efficiency is 100 %. When the Stokes efficiency is close to 100 %, the driving force is close to a constant force (Wang and Oster, 2002). A high Stokes efficiency for the F_1 motor was one of the factors that implicated the progressive binding of ATP as the force-generating process, for only in this fashion could a constant torque be generated (Oster and Wang, 2000).

To summarize, if the thermodynamic efficiency, η_{TD}, is close to 1, this means that the motor motion is *tightly coupled* to the chemical reaction. However, when the Stokes efficiency, $\eta_{Stplers}$, is close to 1, this means that the motor is delivering a nearly *constant force*. Since the Stokes and thermodynamic efficiencies measure different properties of the motor, it is worthwhile to measure both efficiencies experimentally.

8.7 Discussion

The basic principle underlying force generation in molecular motors seems at first glance pretty simple: proteins use short range attractive intermolecular forces to bias small thermal fluctuations or to rectify larger diffusions. The former we call 'power strokes', the latter 'Brownian ratchets'. But the details are all important, and they are devilishly diverse. At some level of abstraction the operation of a molecular motor can be viewed as the motion of a point moving down a multidimensional free energy surface (Bustamante et al., 2001, Oster and Wang, 2000a, Wang et al., 1998). Indeed, many models *start* from this viewpoint and try and deduce what the laws of physics can say about the general properties of the surface. While useful from the viewpoint of theory, models at this level of abstraction are likely to be unsatisfying to biologists who seek a more mechanistic understanding,

1) $\zeta\langle v\rangle^2$ should not be confused with $\zeta\langle v^2\rangle$. By the equipartition theorem of statistical meachanics, $\zeta\langle v^2\rangle$ equals $\zeta k_B T\, m^{-1}$ at equilibrium, where m is the motor mass. $\zeta\langle v^2\rangle$ is several orders of magnitude larger than $\zeta\langle v\rangle^2$.

akin to how an engineer would understand the design and operation of an automobile motor. This involves dealing with the details of protein structure.

The study of molecular motors, more than most other areas in biology, draws on a diversity of fields. Biochemistry elucidates the kinetics of the energy supplying reactions and thermodynamics establishes constraints on the energetic transactions. Mutation studies isolate the key functional amino acids and mechanical measurements provide criteria that circumscribe possible mechanisms. Finally, microscopy and X-ray crystallography provides the *sine qua non* structures, for it is nearly impossible to deduce how a machine works without knowing what it looks like. However, all of these studies combined cannot produce a mechanistic theory of how motor proteins work; this requires the unifying power of mathematical modeling. For until the operation of a motor can be formulated as equations and solved, our knowledge is, at best, qualitative and uncertain, hardly better than a plausible cartoon that may, or may not, obey the laws of chemistry and physics and in any event cannot be compared quantitatively with experiments.

Appendix

A1
Example Models to Illustrate the Difference between Ratchets and Power Strokes

Here we discuss four model examples to illustrate the role of Brownian fluctuations and the classification of power strokes and Brownian ratchets. For simplicity, we consider the one-dimensional motion of an object.

A1.1
Example 1: A power stroke without Brownian fluctuations

Suppose the object is *deterministically* moved forward a fixed unit distance, Δx, per unit time, Δt (e. g. 0.01 nm in 1 μs). The trajectory of the object is shown in Fig. A1a. The object moves forward uniformly with a velocity of $(\Delta x)/(\Delta t)$.

This model example is a pure power stroke without Brownian fluctuations. It is mostly relevant for macroscopic motors. Because of the large inertia, macroscopic motors tend to move at a roughly constant velocity and the effect of Brownian fluctuations is negligible. For protein motors, because of the small size, at room temperature the motion is dominated by Brownian fluctuations. One may argue that this is a hypothetical example of a power stroke protein motor at zero temperature.

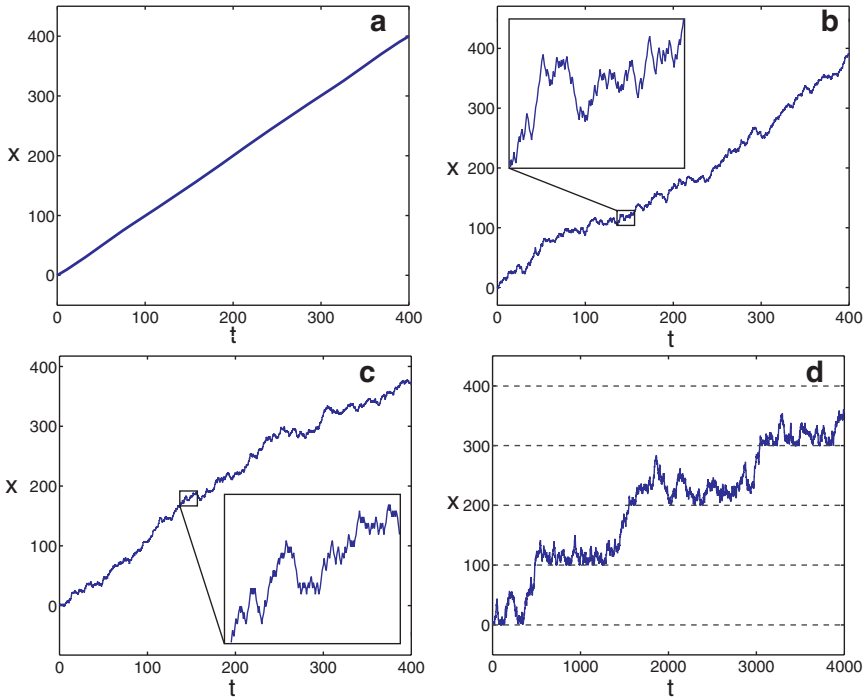

Figure A1. (a) Trajectory of the object for model 1. The object moves forward uniformly with an average velocity of $\langle v \rangle = \Delta x/\Delta t = \Delta x/1$. (b) Trajectory of the object for model 2. The object is driven by a constant force and is subject to Brownian fluctuations. The average velocity of the object is $\langle v \rangle = \Delta x/\Delta t$. (c) Trajectory of the object for model 3. The object is moved by Brownian fluctuations, and the net drift comes from biasing fluctuations. The average velocity of the object is $\langle v \rangle = 0.92 \cdot \Delta x/\Delta t$. The free energy consumption per unit length is the same as that in Example 2. Examples 2 and 3 have similar statistical behaviors, and so it is experimentally difficult to distinguish between them. (d) Trajectory of the object for model 4. The object is moved by Brownian fluctuations, and the net drift comes from rectifying large fluctuations. The free energy consumption per unit length is the same as that in Examples 2 and 3 but the average velocity of the object is $\langle v \rangle = 0.1\ \Delta x/\Delta t$, significantly lower than that of Examples 2 and 3.

Since protein motors can only function in a certain temperature range and in a certain fluid medium, this model is not really relevant for protein motors, and so we must modify it to incorporate Brownian fluctuations.

A1.2
Example 2: A power stroke with Brownian fluctuations

Suppose, in addition to the deterministic unit forward displacement per unit time, in each unit time the object makes $n = 10$ *independent random* moves. Each random move is one unit displacement either forward or backward with equal prob-

ability, p (e. g. flipping a fair coin: $p = 0.5$). This random motion is added to simulate Brownian fluctuations. The trajectory of the object is shown in Fig. A1b. The average velocity of the object is $\langle v \rangle = \Delta x/\Delta t$, but the motion is stochastic. If we view the displacement in each unit time as the 'instantaneous velocity' for that unit time, then *the instantaneous velocity is much larger than the average velocity*. The inset shows the details of the trajectory; it is evident that the deterministic drift is buried in the random motions and can be detected only by looking at long time correlations.

The number of random moves per unit time is proportional to the diffusion coefficient, D, of the object: $2D\Delta t = n(\Delta x)^2$. This allows us to calculate the diffusion coefficient from which the drag coefficient, ζ, is computed from the Einstein relation: $\zeta = k_BT/D$. In this example, the constant force driving the deterministic forward motion is $f = \zeta\langle v \rangle$ and the free energy consumption per unit length is $\zeta\langle v \rangle \Delta x$. For $n = 10$, the free energy consumption per unit length is 0.2 k_BT. A model such as this is appropriate for describing a charged object, such as a DNA strand, driven through a fluid medium by an electrical potential gradient.

A1.3
Example 3: A Brownian ratchet that biases fluctuations

In the two examples above, the net drift is caused directly by a driving force (e. g. an electric potential gradient), and the Brownian fluctuations do not affect the net drift. Next, we consider situations where the net drift is actually caused by biasing or rectifying Brownian fluctuations. In the absence of other influences, the forward and backward fluctuations have the same probability. However, if *internal barriers* are established to block, partially or completely, the backward fluctuations, then the object is more likely to fluctuate forward.

Suppose in each unit time, Δt, the object makes 10 independent random moves (fluctuations). Each random move is 1 unit displacement, Δx, either forward or backward with equal probability ($p = 0.5$). Suppose that each time the object passes a multiple of $5 \times \Delta x$, a barrier is established at that location. At a barrier, the object can fluctuate forward in two ways: a forward Brownian fluctuation and a backward Brownian fluctuation that is reflected by the barrier. The object can move back past the barrier only if a backward Brownian movement 'breaks' the barrier. The probability of breaking a barrier depends on the strength of the barrier. Let p_f be the probability of forward fluctuation at the barrier and p_b be that of backward fluctuation. $\Delta G/k_BT = \log(p_f/p_b)$ gives the free energy (in units of k_BT) required to break the barrier.

If we use $p_f = 0.73$ and $p_b = 0.27$, the corresponding free energy drop at the barrier is 1 k_BT. Since the barriers are separated by $5 \times \Delta x$, the free energy consumption per unit length is $1/5 = 0.2$ k_BT, the same as that used in Example 2. The trajectory of the object is shown in Fig. A1c. The average velocity of the object is $\langle v \rangle = 0.92 \times \Delta x/\Delta t$, similar to Example 2. Because of the small free energy drop (1 k_BT) associated with each barrier, it only partially blocks backward fluctuations.

The inset shows the details of the trajectory. This model is an example of a Brownian ratchet that *biases small fluctuations. The motion of the object is stochastic and indistinguishable from that of Example 2 where the object is driven by a constant force and subject to Brownian fluctuations.*

In this example, the object is directly moved by Brownian fluctuations. The net drift results from biasing fluctuations. For this reason, this model can be classified as a Brownian ratchet. However, it has the same phenomenological behavior as the power stroke motor in Example 2, and so it is very difficult – and unnecessary – to experimentally distinguish it from a power stroke motor.

A1.4
Example 4: A Brownian ratchet that rectifies fluctuations

Finally, consider the model Example 3, but now suppose that in each unit time, Δt, the object makes 10 independent random moves (fluctuations). Each random move is one unit displacement, Δx, either forward or backward with equal probability ($p = 0.5$). Now suppose that each time the object passes a multiple of $100 \times \Delta x$, a barrier of 20 k_BT is established at that location. The barrier is very high: the probability of a forward fluctuation is $p_f = 1 - 3.8 \times 10^{-11} \approx 1$ and the probability of a backward fluctuation that surmounts the barrier is $p_b = 3.8 \times 10^{-11} \approx 0$. Since the barriers are $100 \times \Delta x$ apart, the free energy consumption per unit length is $20/100 = 0.2\ k_BT$, the same as that in Examples 2 and 3. The trajectory of the object is shown in Fig. A1d. The average velocity of the object is $\langle v \rangle = 0.1\Delta x/\Delta t$, significantly lower than that of Examples 2 and 3. Because of the large free energy drop associated with each barrier, it almost completely blocks backward fluctuations. Thus, this model is a Brownian ratchet that *rectifies large fluctuations*. The stochastic motion of the object is different from that of Examples 2 and 3. The object advances *slowly* in *large* ratchet steps: once it passes a multiple of $100\Delta x$, it almost never goes back.

One can add a 'load' to the above examples by decreasing the probability of a forward fluctuation and increasing that of a backward fluctuation at *every* location. One can also combine the power stroke and ratchet by adding both a deterministic motion and larger barriers, or alternatively by adding both small barriers and larger barriers. But this would complicate the model and obscure the simplicity of the distinctions we are trying to illustrate. However, we should point out that there is a way to use the time series data itself to estimate how much of the motor driving force can be ascribed to ratchet and power stroke contributions. This involves constructing an *Effective Driving Potential* from the time series data of the motor; this is discussed in Wang and Oster (2002).

A2
A Closer Look at Binding Free Energy

The simple description given in the text of ATP binding to the catalytic site of F_1 or of ions binding to the rotor of F_0, conceals a great deal of complexity because it neglects the role of solvent effects. Charges in aqueous solution are always hydrated, surrounded by a shifting cohort of hydrogen bonded waters. Before ATP can bind to the catalytic site to initiate the hydrolysis cycle (or sodium binding to the rotor charge in the F_0 motor cycle), both must shed their water coats. The shedding of the water coats is progressive as the hydrogen bonds form between ATP and the catalytic site. Before each hydrogen bond can form, the hydration

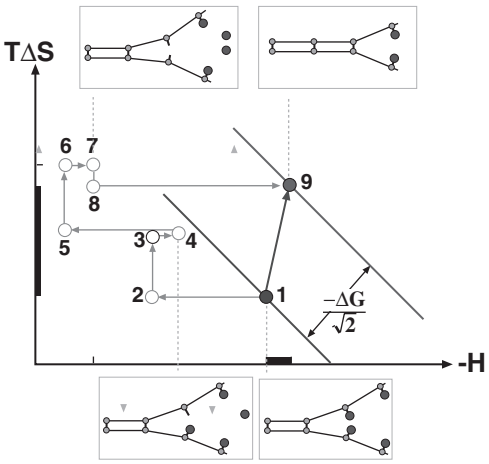

Figure A2. Enthalpic and entropic changes during desolvation and binding can be followed by plotting - ΔH, vs. $T\Delta S$. In these coordinates, the free energy change, ΔG, is plotted as linear contour lines decreasing up and to the right. The formation of one hydrogen bond between the enzyme and nucleotide can be represented schematically as a reversible path showing a single desolvation and binding process. In state 1, the enzyme and nucleotide sites are hydrated (solid circles). Removing a water molecule from one site entails an enthalpic increase, ΔH_{12}. This is followed by an entropic increase, $T\Delta S_{23}$, as the water escapes into solution. Finally, the removed water hydrogen bonds with other waters resulting in an enthalpic decrease, ΔH_{34}. Similar changes accompany the release of a water molecule from the other site during the transition from state 4 to state 7. Now the two empty sites must be brought close together, entailing an entropic decrease, $T\Delta S_{78}$, and an enthalpic decrease, ΔH_{89} as the sites bind. Thus the overall free energy change, ΔG_{19}, has enthalpic and entropic components (black bars) that depend on many factors, especially whether the water binds more strongly to the sites than to other waters. Note that the sequence $1 \rightarrow 9$ is only meant to show the enthalpic and entropic changes. It does not represent the actual sequence of what occurs during the desolvation and binding process. In particular, $2 \rightarrow 3$ (the removed water diffusing into solution) and $3 \rightarrow 4$ (the removed water bonding with other waters) occur simultaneously and cannot be separated.

water molecules must be shed from the donor and receptor just before they form the bond (otherwise they will be re-hydrated quickly). Consider the overall process of the formation of one hydrogen bond between ATP and the catalytic site. This entails a number of energetic and entropic transactions. We can plot the process schematically as the path shown in Fig. A2. (This path does not represent the actual non-equilibrium process, but rather a 'reversible work' path to illustrate the separate entropic and enthalpic transactions). We see that, even in the simplest case, a single association event entails four enthalpic and four entropic changes when water molecules break their hydrogen bonds to charged sites, escape into solution, re-bond with other waters, and finally two sites associate. Clearly, solvent effects can tip the free energy balance, but it is seldom easy to compute how.

The binding transition that generates the power stroke as embodied in Eq. 8.2 and Fig. 8.3 is also an oversimplified description. The hydrogen bonds are not arrayed in a linear sequence (as suggested by the term 'binding zipper'), nor are they either 'on' (zipped) or 'off' (unzipped). The bonding surfaces are complex, hydrogen bonds have a finite range and angular dependence, and thermal motions create a stochastic pattern of graded bonding interactions. Nevertheless, molecular dynamics studies demonstrate that the free energy changes gradually and nearly linearly as the nucleotide unbinds or binds to the catalytic site.

References

Bockmann, R. 2002. Nanoseconds molecular dynamics simulation of primary mechanical energy transfer steps in F1-ATP synthase. *Nat. Struct. Biol.* 9: 198–202.

Bustamante, C., et al. 2001. The physics of molecular motors. *Acc. Chem. Res.* 34: 412–420.

Dimroth, P., et al. 1999. Energy transduction in the sodium F-ATPase of *Propionigenium modestum*. *Proc. Natl. Acad. Sci. USA* 96: 4924–4929.

Hancock, W. and J. Howard. 1999. Kinesin's processivity results from mechanical and chemical coordination between the ATP hydrolysis cycles of the two motor domains. *Proc. Natl Acad. Sci. USA* 96: 13147–13152.

Israelachvili, J. and B. Ninham. 1977. Intermolecular forces – the long and short of it. *J. Colloid Interface Sci* .58: 14–25.

Junge, W., et al. 2001. Inter-subunit rotation and elastic power transmission in F_0F_1-ATPase. *FEBS Lett.* 251: 1–9.

Mahadevan, L. and P. Matsudaira. 2000. Motility powered by supramolecular springs and ratchets. *Science* 288: 95–99.

Menz, R., et al. 2001. Structure of bovine mitochondrial F1-ATPase with nucleotide bound to all three catalytic sites: implications for the mechanism of rotary catalysis. *Cell* 106: 331–341.

Mogilner, A. and G. Oster. 1996a. Cell motility driven by actin polymerization. *Biophys. J.* 71: 3030–3045.

Mogilner, A. and G. Oster. 1996b. The physics of lamellipodial protrusion. *Euro. Biophs. J.* 25: 47–53.

Oster, G. and H. Wang. 2000a. Reverse engineering a protein: The mechanochemistry of ATP synthase. *Biochim. Biophys. Acta* 1458: 482–510.

Oster, G. and H. Wang. 2000. Why is the efficiency of the F1 ATPase so high? *J. Bioenerg. Biomembr.* 332: 459–469.

Oster, G., et al. 2000. How F_0-ATPase generates rotary torque. *Proc. Roy. Soc.* 355: 523–528.

Pedersen, P., et al. 2000. ATP Synthases in the year 2000: evolving views about the structures of these remarkable enzyme complexes. *J. Bioenerget. Biomembr.* 32: ■ ■ ■

Peskin, C. S. and G. Oster. 1995. Coordinated hydrolysis explains the mechanical behavior of kinesin. *Biophys. J.* 68: 202s–210s.

Stock, D., et al. 2000. The rotary mechanism of ATP synthase. *Curr. Opin. Struct. Biol.* 10: 672–679.

Sun, S., et al. 2002. Elastic energy storage in F_1-ATPase. *Proc Nat Acad Sci* ■ ■ ■

Uemura, S., et al. 2002. Kinesin–microtubule binding depends on both nucleotide state and loading direction. *Proc. Natl Acad. Sci. USA* 99: 5977–5981.

Wang, H. and G. Oster. 1998. Energy transduction in the F1 motor of ATP synthase. *Nature* 396: 279–282.

Wang, H. and G. Oster. 2001. The Stokes efficiency for molecular motors and its applications. *Europhys. Lett.* 57: 134–140.

Wang, H. and G. Oster. 2002a. Ratchets, power strokes, and molecular motors. *Appl. Phys. A* ■ ■ ■

Wang, H. and G. Oster. 2002b. The Stokes efficiency for molecular motors and its applications. *Europhys. Lett.* 57: 134–140.

Wang, H., et al. 1998. Force generation in RNA polymerase. *Biophys. J.* 74: 1186–1202.